Neutron diffraction study on phase transition and thermal expansion of SrFeAsF

Y. Xiao,[1,*] Y. Su,[2] R. Mittal,[2,3] T. Chatterji,[4] T. Hansen,[5] S. Price,[2] C. M. N. Kumar,[1] J. Persson,[1] S. Matsuishi,[6] Y. Inoue,[6] H. Hosono,[6] and Th. Brueckel[1,2,4]

[1]*Institut fuer Festkoerperforschung, Forschungszentrum Juelich, D-52425 Juelich, Germany*
[2]*Juelich Centre for Neutron Science, IFF, Forschungszentrum Juelich, Outstation at FRM II, Lichtenbergstrasse 1, D-85747 Garching, Germany*
[3]*Solid State Physics Division, Bhabha Atomic Research Centre, Trombay, Mumbai 400 085, India*
[4]*Juelich Centre for Neutron Science, IFF, Forschungszentrum Juelich, Outstation at Institut Laue-Langevin, BP 156, 38042 Grenoble Cedex 9, France*
[5]*Institut Laue-Langevin, BP 156, 38042 Grenoble Cedex 9, France*
[6]*Frontier Research Center, Tokyo Institute of Technology, 4259 Nagatsuta-cho, Midori-ku, Yokohama 226-8503, Japan*

(Dated: December 8, 2009)

The magnetic ordering and crystal structure of iron pnictide SrFeAsF was investigated by using neutron powder diffraction method. With decreasing temperature, the tetragonal to orthorhombic phase transition is found at 180 K, while the paramagnetic to antiferromagnetic phase transition set in at 133 K. Similar to the parent compound of other iron pnictide system, the striped Fe magnetism is confirmed in antiferromagnetic phase and the Fe moment of 0.58(6) μ_B aligned along long *a* axis. The thermal expansion of orthorhombic phase of SrFeAsF is also investigated. Based on the Grüneisen approximation and Debye approximation for internal energy, the volume of SrFeAsF can be well fitted with Debye temperature of 347(5) K. The experimental atomic displacement parameters for different crystallographic sites in SrFeAsF are analyzed with Debye model. The results suggested that the expansion of FeAs layers plays an important role in determining the thermal expansion coefficient.

PACS numbers: 74.70.Xa, 75.25.-j, 65.40.De

High temperature superconductivity has recently been discovered in carriers doped iron pnictide compounds [1, 2, 3, 4]. Till now, the highest T_c attained is 57.4 K in the electron doped '1111' compound $Ca_{0.4}Na_{0.6}FeAsF$ [5], while for the so called '122' compound the highest T_c of 38 K is reached in the hole doped $Ba_{0.6}K_{0.4}Fe_2As_2$ [4]. It is generally believed that the superconductivity in iron pnictides is unlikely due to simple electron-phonon coupling, as demonstrated from extensive studies of phonon dynamics [6, 7]. Magnetism seems to play a crucial role in the appearance of superconductivity and AFM spin fluctuations have thus been suggested to be a possible pairing mechanism [8].

The spin density wave (SDW) transition, which is associated with long range antiferromagnetic (AFM) order of Fe moments, is shown in undoped FeAs-based compounds [9, 10, 11, 12]. Band structural calculations suggested that the SDW is driven either by Fermi surface nesting between electron and hole pockets or by the magnetic exchange coupling between local moments [13, 14, 15, 16]. Furthermore, the SDW transition is found to be accompanied by the tetragonal to orthorhombic (T-O) structural phase transition in the 122 family and preceded by the T-O transition for the 1111 family [9, 10, 11, 12]. It is generally accepted that the crystal and magnetic structure in undoped FeAs compound are intimately coupled. Theoretical studies suggested that the structural phase transition is driven by the AFM stripe magnetism directly [14, 16, 17]. Therefore, it is important to investigate the relationship between structural properties and AFM ordering of the undoped FeAs compound, especially for the 1111 compound, in which the structural phase transition always occurred at higher temperature than SDW transition temperature.

As a new parent phase of iron pnictide family, the SrFeAsF also exhibited prominent anomaly in magnetic and electric property measurements [18, 19, 20]. However, detailed studies have not been carried out to investigate the magnetic and structural transformation in SrFeAsF. In this paper, we investigated the structural and magnetic phase transition as well as thermal expansion in SrFeAsF compound by using the neutron powder diffraction (NPD) method. Both structural and magnetic phase transitions are clarified; the temperature dependence of atomic displacement parameters and thermal expansion are well modeled based on the experimental results. The SrFeAsF polycrystalline sample was synthesized by a solid state reaction method as described in Ref [18] with impurity phases (CaF_2 and Fe_2O_3) of less than 1%. The neutron powder diffraction measurements were performed on the high flux powder diffractometer D20 at Institut Laue Langevin (Grenoble, France). A Ge (115) monochromator was used to produce a monochromatic neutron beam of wavelength 1.88 Å. The sample was loaded in a vanadium sample holder and then installed in the liquid helium cryostat that can generate temperature down to 2 K. The program FULLPROF [21] was used for the Rietveld refinement of the crystal and the magnetic structures of the compounds.

Similar to the CaFeAsF compound, the SrFeAsF also crystallized in orthorhombic structure with space group *Cmma* at 2 K. Refinement of the neutron diffraction pattern gave lattice parameters of a = 5.6689(1) Å, b = 5.6260(1) Å and c = 8.9325(2) Å at 2 K. Both lattice parameters and unit-cell

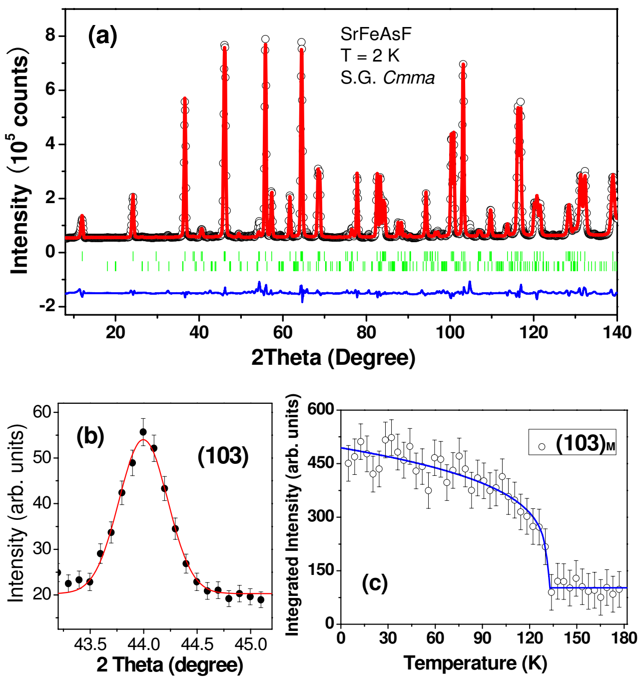

FIG. 1: (Color online) (a)Neutron powder diffraction pattern of SrFeAsF at 2 K. The cirlces represent the observed intensities, the solid line is the calculated pattern. The difference between the observed and calculated intensities is shown at the bottom. The vertical bars indicate the expected nuclear and magnetic Bragg reflection positions. (b) The $(103)_M$ magnetic reflections obtained by subtracting the NPD pattern measured at 240 K from the pattern measured at 2 K. (c) Temperature dependence of the integrated intensity of $(103)_M$ magnetic Bragg reflection. The solid curve is fit to the power law.

volume V are larger than that in CaFeAsF, which is consistent with the fact that the atomic radius of Sr is larger than that of Ca. The refined neutron powder diffraction pattern of SrFeAsF at 2 K is shown in Fig. 1(a). Apart from the nuclear Bragg reflections, the magnetic peaks can be fitted by using the same AFM structural model as in CaFeAsF [22] for Fe magnetism and the Fe moment is deduced to be 0.58(6) μ_B. It seems that the AFM configuration of Fe spins and the small magnitude of moment are a common feature for all FeAs systems. The origin of that small iron moment in these compounds was explained theoretically as the result of the itinerant character of iron spins [13] or the nearest and next nearest neighbor superexchange interactions between Fe ions which give rise to a frustrated magnetic ground state [14]. The temperature dependence of integrated intensity of $(103)_M$ magnetic reflection was plotted in Fig. 1(c) to obtain the AFM phase transition temperature. By fitting the ordering parameter with power law, the Fe spins are found to order below T_N = 133(3) K. The onset of the structural phase transition from *P4/nmm* to *Cmma* takes place at T_S = 180(2) K as indicated by the evolution of $(220)_O$ tetragonal reflection with temperature [Fig. 2(a)]. The T_S is in accordance with the structural phase transition observed by other methods [18, 19, 20].

The variation of lattice parameters can be obtained through

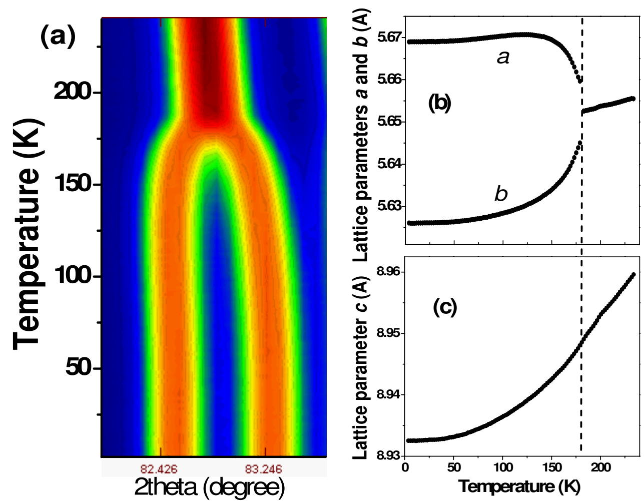

FIG. 2: (Color online) (a) Evolution of $(220)_T$ reflections with the change of temperature. The structural phase transition is clearly revealed by the splitting of tetragonal $(220)_T$ into orthorhombic $(400)_O$ and $(040)_O$ reflections. (b)(c) Temperature dependence of the estimated lattice parameter a, b and c for both tetragonal and orthorhombic phases.

the refinement of NPD patterns. As shown in Fig. (b) and (c), the lattice parameters a and b deviated each other when the temperature is lower than the structural phase transition temperature, while the lattice parameter c decreased gradually with decrease of temperature. The structural distortion will result in an inequivalent of nearest- and next-nearest-neighbor coupling (J_1 and J_2) in FeAs layers and lift the magnetic frustration. The collinear AFM spin configuration is stabilized as the ground state when $J_2 > J_1/2$ [14, 16]. Within the Heisenberg magnetic exchange model, it is established that the difference between the structural and AFM transition temperature is strongly correlated with the ratio between out-of-plane magnetic exchange coupling J_z and J_2 [16, 23]. To our knowledge, the difference between T_S and T_N in SrFeAsF ($\sim$ 47 K) is the largest among all known iron pnictides. Therefore, the big temperature difference between T_s and T_N indicates the smallest J_z/J_2 ratio in SrFeAsF.

The detailed structural information for SrFeAsF at 2 K and 240 K, as obtained from NPD data, are given in Table I. The variation of volume with temperature over measured temperature range is shown in Fig. 3. To model the experimental data of the unit cell volume, we followed the approach of the Grüneisen approximation for the zero pressure equation of state, in which the effects of thermal expansion are considered to be equivalent to elastic strain [24]. Thus, the temperature dependence of the volume can be described by $V(T) = \gamma U(T)/K_0 + V_0$, where γ is a Grüneisen parameter, K_0 is the incompressibility and V_0 is the volume at T = 0 K. By adopting the Debye approximation, the internal energy $U(T)$ is given by:

$$U(T) = 9Nk_BT\left(\frac{T}{\theta_D}\right)^3 \int_0^{\theta_D/T} \frac{x^3}{e^x - 1}\mathrm{d}x \tag{1}$$

TABLE I: Refined results of the crystal and magnetic structures for SrFeAsF at 2 and 240 K. The atomic positions for space group *Cmma*: Sr(4*g*)(0,0.25,z), Fe(4*b*)(0.25,0,0.5), As(4*g*)(0,0.25,z), F(4*a*)(0.25,0,0); for *P4/nmm*: Sr(2*c*)(0.25,0.25,z), Fe(2*b*)(0.75,0.25,0.5), As(2*c*)(0.25,0.25,z), F(2*a*)(0.75,0.25,0).

Temperature	2 K	240 K
Space group	*Cmma*	*P4/nmm*
a (Å)	5.6689(1)	3.9996(1)
b (Å)	5.6260(1)	3.9996(1)
c (Å)	8.9325(2)	8.9618(4)
V (Å^3)	284.89(2)	143.36(2)
Sr		
z	0.1584(1)	0.1583(2)
B(Å^2)	0.05(4)	0.44(4)
Fe		
B(Å^2)	0.04(2)	0.29(2)
$M_a(\mu_B)$	0.58(6)	
As		
z	0.6525(1)	0.6515(1)
B(Å^2)	0.05(4)	0.33(4)
F		
B(Å^2)	0.13(3)	0.38(3)
Bondlength(Å)		
Fe-Fe	2.834(2)×2 2.813(1)×2	2.828(2)×4
Fe-As	2.417(2)×4	2.417(2)×4
Bondangle(°)		
Fe-As-Fe	71.168(3)×2 71.794(3)×2 111.394(3)×2	71.608(3)×4 111.653(3)×2
R_p	3.43	4.98
R_{wp}	5.09	7.58
χ^2	3.53	5.63

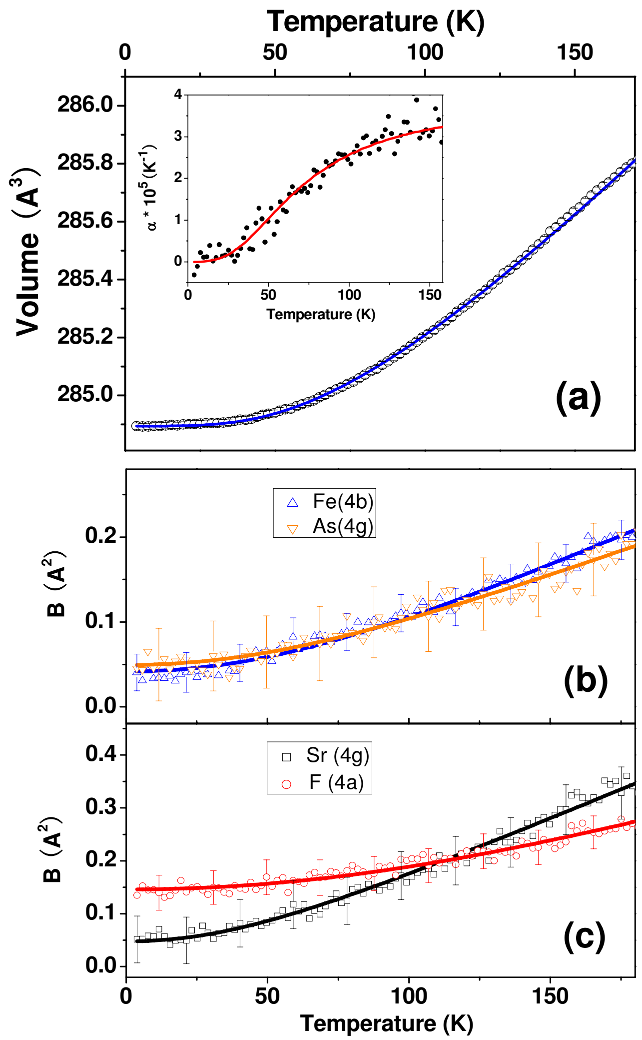

FIG. 3: (Color online) (a) Temperature dependence of the volume of unit cell of SrFeAsF. The solid line is fit of the Debye model as described in the text. The inset shows the thermal expansion constant of volume as determined from the fit of the Debye model in comparison to the experimental data. (b)(c) Isotropic thermal parameters for different atomic sites in SrFeAsF.

where N is the number of atoms in the unit cell, k_B is the Boltzmann's constant and θ_D is the Debye temperature. Above model exhibits a good fit to volume variation as indicated by the solid line in Fig. 3. We obtained following physical parameters: θ_D = 347(5) K, V_0 = 284.89(2) Å^3 and γ/K_0 = 1.57(3)×10^{-9} Pa^{-1}. The value for the Debye temperature as determined from neutron experiments is in reasonable agreement with those determined from specific heat measurements, θ_D = 339(1) in Ref[19]. Note that the Debye temperature approximates only the acoustical phonons at low temperature. The thermal expansion coefficient $\alpha(T)$ which corresponds to the first derivative of $U(T)$ divided by the unit cell volume at that temperature is plotted in the inset of Fig. 3(a) as the solid dots. The solid curve correspond to the calculated value of $\alpha(T)$ from $V(T)$.

As a basic crystallographic parameter, the atomic displacement parameter (ADP) can reflect the atomic thermal motion and provide useful information on the thermal properties of materials [25, 26]. Therefore, the ADPs of different crystallographic sites in SrFeAsF was also investigated. For the low temperature *Cmma* phase, the space group symmetries of all special positions [Sr(4*g*), Fe(4*b*), As(4*g*) and F(4*a*)] allow three independent ADP elements. Based on approximate classification, the isotropic ADP $\langle U^2_{iso}\rangle$ was applied by assuming that the displacements are the same in all directions. The thermal parameter B_{iso} which is obtained assuming isotropic thermal motions of atoms are evaluated using the relation B_{iso} = $8\pi^2\langle U^2_{iso}\rangle + B_{sta}$, where B_{sta} is the static component of the thermal parameter caused by the presence of a certain amount of static disorder in compounds. Fig. 3(b) and Fig. 3(c) show the temperature variation of experimental thermal parameters for all four atomic sites of SrFeAsF. Debye model was adopted to describe the ADP as a function of temperature:

$$\langle U^2_{iso}\rangle = \frac{3\hbar^2 T}{mk_B\theta_D^2}\left(\Phi(\theta_D/T) + \frac{\theta_D}{4T}\right) \qquad (2)$$

where $\Phi(\theta_D/T)$ is given by

$$\Phi(\theta_D/T) = \frac{T}{\theta_D}\int_0^{\theta_D/T}\frac{x}{e^x-1}\mathrm{d}x \quad (3)$$

The fitted results for the thermal parameters based on above equations are plotted in Fig. 3(b) and Fig. 3(c) as the solid lines in comparison with the experimental results. The Debye temperatures evaluated for different atomic species are Sr [238(6)K], Fe [365(6)K], As [348(6)K] and F [611(6)K]. The averaged mass weighted value for the Debye temperature is obtained to be 332(10) K. The corresponding Debye frequencies for Sr, Fe, As, F sites are 4.9(1), 7.6(1), 7.2(1) and 12.7(1) THz respectively. The small difference between the Debye frequencies for Fe and As revealed the similar range of phonon frequencies for those two sites. The range of phonon frequencies obtained from our analysis is in very good agreement with our recent inelastic neutron scattering and *ab initio* phonon calculation results [27] for SrFeAsF indicating the reliability of our analysis.

ab initio electronic structure calculations for SrFeAsF [28] shows that it possessed essentially the same band dispersions in the vicinity of the Fermi surface as in other 1111 compounds, such as LaFeAsO and CaFeAsF. Furthermore, the electronic states near the Fermi surface are dominated by contributions from Fe and As, which indicates that the FeAs layers are playing an important role in magnetism and superconductivity of the compound. From our thermal parameter analysis, we also notice that the mean value of the Debye temperature for Fe and As [355(8) K] in SrFeAsF agrees well with the Debye temperature deduced from the analysis of thermal expansion curve [Fig. 3(a), θ_D = 347(5) K]. Therefore, the thermal expansion of FeAs layers is supposed to be the main contribution to the thermal expansion of volume.

In summary, the structural and magnetic phase transition as well as the thermal expansion of SrFeAsF was investigated by using the neutron diffraction method. The onset of tetragonal to orthorhombic phase transition is at 180 K while the paramagnetic to antiferromagnetic phase transition takes place at 133 K. SrFeAsF exhibites the largest difference between T_S and T_N among all known iron pnictides. The striped AFM arrangement of Fe spins is confirmed by refinement of neutron data. The magnitude of Fe moment aligned along *a* direction is deduced to be 0.58(6) μ_B. The lattice volume of low temperature orthorhombic phase can be modeled well in frame of Grüneisen approximation with a Debye approximation for the internal energy. The analysis on atomic displacement parameters of different crystallographic sites suggested that the vibration of Fe and As is coupled in FeAs layers and they contribute mainly to the thermal expansion of volume in SrFeAsF.

* y.xiao@fz-juelich.de

[1] Y. Kamihara, T. Watanabe, M. Hirano, and H. Hosono, J. Am. Chem. Soc. **130**, 3296 (2008).

[2] X. H. Chen, T. Wu, G. Wu, R. H. Liu, H. Chen, and D. F. Fang, Nature (London) **453**, 761 (2008).

[3] H. Takahashi, K. Igawa, K.Arii, Y. Kamihara, M. Hirano, and H. Hosono, Nature (London) **453**, 376 (2008).

[4] M. Rotter, M. Tegel, and D. Johrendt, Phys. Rev. Lett. **101**, 107006 (2008).

[5] Peng Cheng, Bing Shen, Gang Mu, Xiyu Zhu, Fei Han, Bin Zeng, and Hai-Hu Wen, Europhys. Lett. **85**, 67003 (2009).

[6] R. Mittal, Y. Su, S. Rols, T. Chatterji, S. L. Chaplot, H. Schober, M. Rotter, D. Johrendt, and Th. Brueckel, Phys. Rev. B **78**, 104514 (2008).

[7] R. Mittal, M. Zbiri, S. Rols, Y. Su, Y. Xiao, H. Schober, S. L. Chaplot, M. Johnson, T. Chatterji, S. Matsuishi, H. Hosono, and Th. Brueckel, Phys. Rev. B **79**, 214514 (2009).

[8] A. D. Christianson, E. A. Goremychkin, R. Osborn, S. Rosenkranz, M. D. Lumsden, C. D. Malliakas, I. S. Todorov, H. Claus, D. Y. Chung, M. G. Kanatzidis, R. I. Bewley and T. Guidi, Nature **456**, 930 (2008).

[9] C. de la Cruz, Q. Huang, J. W. Lynn, J. Li, W. Ratcliff II, J. L. Zarestky, H. A. Mook, G. F. Chen, J. L. Luo, N. L. Wang, and P. C. Dai, Nature (London) **453**, 899 (2008).

[10] J. Zhao, Q. Huang, C. de la Cruz, S. Li, J. W. Lynn, Y. Chen, M. A. Green, G. F. Chen, G. Li, Z. Li, J. L. Luo, N. L. Wang, and P. Dai, Nature Materials **7**, 953 (2008).

[11] Q. Huang, Y. Qiu, W. Bao, J.W. Lynn, M. A. Green, Y. Chen, T. Wu, G. Wu, and X. H. Chen, Phys. Rev. Lett. **101**, 257003 (2008).

[12] Y. Su, P. Link, A. Schneidewind, Th. Wolf, Y. Xiao, R. Mittal, M. Rotter, D. Johrendt, Th. Brueckel, and M. Loewenhaupt, Phys. Rev. B **79**, 064504 (2009).

[13] I. I. Mazin, D. J. Singh, M. D. Johannes, and M. H. Du, Phys. Rev. Lett. **101**, 057003 (2008).

[14] T. Yildirim, Phys. Rev. Lett. **101**, 057010 (2008).

[15] Q. M. Si and E. Abrahams, Phys. Rev. Lett. **101**, 076401 (2008).

[16] C. Fang, H. Yao, W. F. Tsai, J. P. Hu, and S. A. Kivelson, Phys. Rev. B **77**, 224509 (2008).

[17] I. I. Mazin and M. D. Johannes, Nature Physics **5**, 141 (2009).

[18] Satoru Matsuishi, Yasunori Inoue, Takatoshi Nomura, Masahiro Hirano and Hideo Hosono, J. Phys. Soc. Jpn. **77**, 113709 (2008).

[19] M. Tegel, S. Johansson, V. Weiss, I. Schellenberg, W. Hermes, R. Poettgen, and D. Johrendt, Europhys. Lett. **84**, 67007(2008).

[20] Fei Han, Xiyu Zhu, Gang Mu, Peng Cheng, and Hai-Hu Wen, Phys. Rev. B **78**, 180503 (2008).

[21] J. Rodriguez-Carvajal, Physica B **192**, 55 (1993).

[22] Y. Xiao, Y. Su, R. Mittal, T. Chatterji, T. Hansen, C.M.N. Kumar, S. Matsuishi, H. Hosono, and Th. Brueckel, Phys. Rev. B **79**, 060504(R) (2009).

[23] Yongkang Luo, Qian Tao, Yuke Li, Xiao Lin, Linjun Li, Guanghan Cao, Zhu-an Xu, Hiroshi Kaneko, Andrey V. Savinkov, Yun Xue, Haruhiko Suzuki, Chen Fang, Jiangping Hu, arXiv:0911.2779.

[24] D. C. Wallace, Thermodynamics of Crystals, Dover, New York, (1998).

[25] R. W. Grosse-Kunstleve and P. D. Adams, J. Appl. Crys. **35**, 477 (2002).

[26] B. C. Sales, B. C. Chakoumakos, D. Mandrus and J. W. Sharp, J. Solid State Chem. **146**, 528 (1999).

[27] R. Mittal et al., in preparation.

[28] I. A. Nekrasov, Z. V. Pchelkina and M. V. Sadovskii, JETP Letters, **88**, 679 (2008).